Monolithic Tunable InAs/InP Broadband Quantum-Dash Laser

EMAD ALKHAZRAJI[1,2], **(Member, IEEE), MOHD SHARIZAL ALIAS**[3], **(Senior Member, IEEE),**
KHURRAM KARIM QURESHI[4], **(Senior Member, IEEE), AND**
MOHAMMED ZAHED MUSTAFA KHAN[1], **(Senior Member, IEEE)**

[1]Optoelectronics Research Laboratory, Electrical Engineering Department, King Fahd University of Petroleum and Minerals, Dhahran 31261, Saudi Arabia
[2]Department of Electrical and Electronic Engineering Technology, Jubail Industrial College, Jubail 31961, Saudi Arabia
[3]Faculty of Engineering Technology and Science, Higher Colleges of Technology, Dubai 15825, UAE
[4]Electrical Engineering Department, King Fahd University of Petroleum and Minerals, Dhahran 31261, Saudi Arabia

Corresponding author: Mohammed Zahed Mustafa Khan (zahedmk@kfupm.edu.sa)

ABSTRACT A two-sectioned quantum dash laser structure based on an InAs/InP chirped active region medium is investigated as a monolithic broadband tunable laser. A thorough parametric analysis on the effect of three tuning parameters (*viz.* injection current, cavity length, absorber-to-device length ratio) on the optical power-injection current (L-I) and spectral characteristics, particularly wavelength tunability and bandwidth broadening, is performed. A total emission wavelength tunability of ∼20 nm is demonstrated in the mid-L-band (∼1600 to ∼1620 nm) window and ∼2 times enhancement in the 3dB bandwidth. Furthermore, optical bistability in the two-sectioned InAs/InP quantum-dash laser device is observed at near room temperature in the form of L-I curve hysteresis. Further investigation displayed a direct relation between the absorber length and the hysteresis loop width with a maximum value of ∼40 mA is demonstrated; a potential platform in fast optical switching and modulation applications. Finally, the two-sectioned structure is also proposed and investigated as a monolithic two-segment contact spectrum shaper to manipulate the lasing spectrum profiles to attain flat tops and effectively increase the spectrum 3dB bandwidth. As such, a maximum 3dB bandwidth was able to be pushed up to ∼20 nm from ∼7 nm by proper tuning of the current density distribution across the two segments of the device.

INDEX TERMS Broadband lasers, quantum-dash lasers, quantum-dot lasers, tunable lasers, multi-segment lasers, two-section lasers, L-band lasers, optical bistability.

I. INTRODUCTION

A tunable optical source, by definition, is one whose emission wavelength can be manipulated or adjusted through different mechanisms. Recently, semiconductor tunable optical sources have become critical components in numerous applications, including bio-medical sensing, hyperspace imaging, nanostructure characterization, process control, and optical access networks [1]. Furthermore, it is believed that tunable semiconductor lasers will be indispensable in next-generation high-scale wavelength division-multiplexed passive optical networks (WDM-PON) that promise to support virtually limitless bandwidth to subscribers at a high degree of scalability

and flexibility in addition to offering bitrate- and protocol-transparency [2]–[7].

Though the tunability of optical sources can be achieved through different mechanisms, monolithic tunable semiconductor sources offer an extra edge over external cavity tuning structures for their compactness, reliability, ease in tuning, and integrability with other optoelectronic components. In such monolithic configurations, the tunability is achieved over a single device either via altering the wavelength selectivity of distributive feedback (DFB) structure [8], employing segmented two or more sections where one acts as a gain medium section while the other(s) acts as a saturable absorber [1], [2], partially-injected section [9], [4], etc. Although the DFB approach yields high-performance tunable devices, however, suffers from the cost issues and

The associate editor coordinating the review of this manuscript and approving it for publication was San-Liang Lee.

hence may pose challenges in future WDM-PON that are expected to exhibit optimized capital and operational expenditures. On the other hand, a two- or multi-section devices approach for wavelength tuning is attractive in meeting these requirements, thanks to their simple and cost-effective design.

As such, several reports have incorporated different monolithic multi-sectioned configurations. In quantum-well active region based laser device structures, for instance, a triple-contact Fabry–Pérot (FP) quantum-well laser diode was adopted in [2], [3] where a total continuous tunability of 6.1 nm was demonstrated in the C-band by controlling the injected currents into the three sections of the device. Tunability was then utilized to counter the junction heating-based wavelength shifts and realize a temperature-independent source in a WDM system. Two-sectioned configurations were also adopted in few reports over quantum-well active structures. For instance, with a two-sectioned InGaAsP/InP FP laser diode, a continuous tunability of 12 nm in the C-band ($\sim$1550 nm) is demonstrated [6]. Moreover, slotted [4], [10] and coupled-cavity [11], [12] InGaAsP/InP and AlGaAlAs/InP multiple-quantum-well laser diodes were also reported to achieve wavelength tunability in the range of 40 nm covering 1555 nm to 1595 nm with the aid of manipulating the junction temperature via a thermoelectric cooler (TEC).

Nevertheless, wavelength tunability was also reported over further low-dimensional active region laser device structures such as two-sectioned mode-locked quantum-dot laser diode with and without the assistance of a TEC, showing a maximum tuning range of 7.7 nm in the C-band [4], [5]. Furthermore, a tunability of 45 nm was also reported over a monolithic multi-sectioned InAs/GaAs quantum-dot laser in $\sim$1245–1290 nm window by employing reverse-bias of one section as the tuning parameter [13].

In the recent years, semiconductor lasers based on InAs/InP quantum dash (Qdash) active region structures have shown outstanding characteristics owing to their mixed quantum-wire and quantum-dot properties, large wavelength tunability spanning C- to U-bands during the growth process, and highly inhomogeneous nature that resulted in ultra-broad lasing emissions. These niche characteristics qualify them as strong contenders for optical sources in next-generation WDM-PONs that are expected to have an extended wavelength coverage penetrating the entire L-band [9].

In this work, we present a thorough experimental investigation of monolithic two-sectioned InAs/InP Qdash semiconductor laser diode based on an exceedingly highly inhomogeneous chirped barrier thickness active region structure. Such analysis is of considerable significance as it provides an in-depth insight into the different parameters in designing and device optimization such as injection current, cavity length, and absorber-to-device length ratio. Our results demonstrated a continuous wavelength tunability of $\sim$20 nm, which is also the largest continuous tunability range in the mid-L-band, to our knowledge. Furthermore, said inhomogeneity also yielded in broadened emission spectrum from
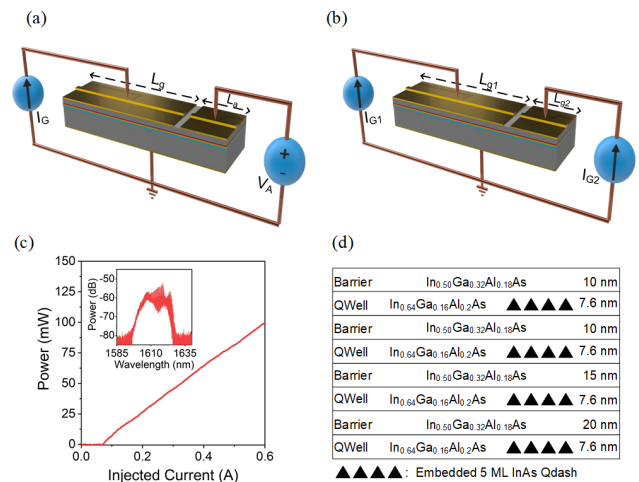

FIGURE 1. Illustration of monolithic two-sectioned (a) QD-LD tunable laser and (b) QD-LD as a spectral shaper, depicting their respective circuit diagram and the biasing sources; pulsed current source (I_G) and DC voltage source (V_A) in (a) and two separate pulsed current sources I_{G1} and I_{G2} in (b). (c) The L-I curve of 760 μm QD-LD when biased as a single section. The inset shows the associated lasing emission spectrum at a current injection of 1.1I_{th}. (d) A schematic diagram of the chirped structure of the active region.

the two-section devices besides tunability, with observed $\sim$2 times bandwidth enhancement.

Near room temperature, optical bistability phenomenon is also observed in such two-section InAs/InP Qdash laser devices, and a comprehensive investigation showed a hysteresis loop in the L-I curve as wide as 40 mA. Finally, we proposed and employed the two-sectioned device as a spectrum shaper by independently altering the current distribution across the two-segments and hence, laser's active medium. As such, a flatter top lasing emission profile was demonstrated, which ultimately resulted in increasing the 3dB bandwidth from $\sim$7 nm to $\sim$20 nm.

II. EXPERIMENTAL SETUP

The device under investigation is an InAs/InP Quantum-dash laser diode (QD-LD) whose lasing emission tunability is realized by segmenting the diode into two isolated sections, as illustrated in Fig. 1(a). The resulting isolation resistance between these two sections was measured to be $\sim$0.4 − 0.6 kΩ over different cavity length QD-LDs, and various lengths of the two segments.

The active region of the QD-LD, on the other hand, is a chirped barrier thickness InAs/InP Quantum-dash structure. The chirped active region consists of four stacks, each comprised of 5 monolayers of InAs dashes embedded within 7.6 nm of strained $In_{0.64}Ga_{0.16}Al_{0.2}$ As asymmetric quantum-wells. Each stack is followed by a tensile-strained $In_{0.50}Ga_{0.32}Al_{0.18}$ As atop barrier layers. The thickness of barrier layers was varied from one stack to the other to increase the structure's inhomogeneity as it has been demonstrated that the barrier layer thickness plays a vital role in determining the size, height in particular, of the grown

subsequent dashes, and hence their corresponding ground-state transition energies [14]. This intentional increase in the inhomogeneity of the active region consequently broadens the active region gain profile. Due to the chirped structure design an intentional inhomogeneity of the active region owing to the self-assembled growth process of quantum-dashes, the laser device demonstrated ultra-broad gain profile and lasing emission spectra at ∼1600 nm.

In this work, two device configurations are studied *viz.* tunable laser and spectral shaper with as-cleaved facets and 3 μm ridge width. For the former case, the longer section acts as a gain section (GS), whereas the other shorter section serves as a saturable absorber section (AS) whose loss is manipulated by reverse-biasing the segment to alter the lasing emission wavelength. Fig. 1(a) shows this configuration with each segment biased via a separate dedicated source. Firstly, a pulsed current source (Keithley 2520) I_G with a duty cycle of 0.2% and a pulse-width of 0.5 μs is used for current injection into the GS. Simultaneously, a direct current (DC) voltage source (Keithley 2400) V_A is employed to reverse bias the AS. On the other front, the spectral shaper device configuration is depicted in Fig. 1(b) wherein the shorter section, in this case, acts as the second gain section GS2 while the longer section is the first gain section GS1 instead of GS.

Moreover, for probing GS2, another pulsed current source (Keithley 2520) I_{G2} with identical current pulse setting is utilized while the source of GS1 remained unaltered. In both the device configurations, the optical power is collected from the AS/GS2 facet and then coupled into a single-mode optical fiber for spectral analysis. For L-I characteristics, a calibrated integrating sphere with InGaAs photodiode is employed to collect the optical power directly from the front AS/GS2 facet. Moreover, single front facet external differential quantum efficiency ($d\eta_d/dI$) of this two-section asymmetric device is also extracted for performance comparison purposes. All the measurements are performed at 14ºC to minimize the effect of junction heating as the device structure is an unoptimized one. It is also worth mentioning here that Q-switching and mode-locking are potentially attainable in these two-sectioned devices [15], [16]; however, the present work is limited to the investigation of monolithic tunable laser and spectral shaper.

III. RESULTS AND DISCUSSION

In this section, we studied the two device configurations mentioned above on the two-sectioned QD-LD, *i.e.,* a monolithic tunable source via altering the loss of the AS, and a monolithic lasing emission spectrum shaper via manipulating the current distribution among the two GS1-GS2 sections.

At first, a QD-LD was selected with a cavity length (L) of 760 μm, a gain section length (L_g) of 660 μm, and an absorber section length (L_a) of 100 μm, hence absorber-to-device length ratio (L_a/L) of ∼13%. Fig. 1(c) shows the L-I curve of the device when both sections are electrically shorted and pumped with a single pulsed current source making the
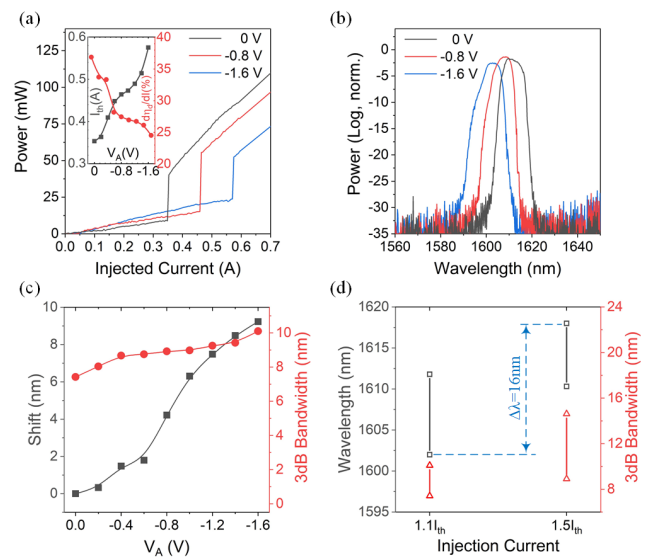

FIGURE 2. (a) The L-I curves of a two-sectioned QD-LD of a cavity length 760 μm under different reverse-bias V_A values and a temperature of 14°C. The inset shows a summary of the variation in Ith and $d\eta_d/dI$ as functions of V_A. (b) The corresponding emission spectra at a current injection of 1.1I_{th} under V_A values of 0, −0.8, and −1.6 V. (c) The blueshift of the central wavelength and 3dB bandwidth exhibited by the lasing spectra as a function of V_A. (d) A summary of the total wavelength tunability and bandwidth broadening under I_G settings of 1.1I_{th} and 1.5I_{th}.

QD-LD to operate as a single-sectioned device. The L-I curve shows a threshold current (I_{th}) of ∼70 mA, and a typical emission spectrum at 1.1I_{th} is depicted in the inset of Fig. 1(c). A measured central wavelength of ∼1616 nm (calculated as the mid-point between the −3 dB points) and a broad 3dB-bandwidth of ∼7.6 nm is noticed. Of course, with increasing in current injection, the 3dB bandwidth is found to broadened considerably.

A. TWO-SECTIONED QD-LD AS A TUNABLE LASER
We start with the investigation of the wavelength tunability of the two-sectioned QD-LD by measuring the L-I and spectral characteristics and after that analyzing the effect of pulsed current injection, the geometrical effects of the two-sections such as the length of the absorber section and the device cavity length, over QD-LD's tuning characteristics. Furthermore, we also shed light on the optical bistability observation at near room temperature in this device, which is, to our knowledge, has not been reported before at near room temperature.

1) EFFECT OF INJECTION CURRENT
To start with, each of the GS and the AS is biased independently with I_G and V_A, respectively, where the latter is varied from 0 V to −1.6 V to tune the central emission wavelength, while the former was swept between 0 and 700 mA to obtain the L-I curves of the two-sectioned QD-LD. Fig. 2(a) depicts the obtained L-I curves for $V_A = 0$, −0.8, and −1.6 V. Several observations can be inferred by analyzing the L-I curves. First, the device witnesses an increase in its threshold current with large negative V_A values whereas its

near-threshold $d\eta_d/dI$ degraded in the form of the observed lower slope efficiency. The inset of Fig. 2(a) summarizes both of these parameters as a function of V_A. In particular, I_{th} increased from ~353 mA to ~575 mA as V_A was swept from 0 V to −1.6 V whereas $d\eta_d/dI$ diminished from ~37% to ~25%. Both trends come as no surprise due to the introduced losses within the AS under higher negative bias values of V_A. This causes additional photon re-absorption (*i.e.,* higher rates of re-absorption) occurrence in the AS, thus lowering $d\eta_d/dI$, in addition to increasing the overall gain threshold (g_{th}) of the device, resulting in raising I_{th} value as well as reducing the total optical power of the system [17].

Furthermore, a sharp turn-on behavior (in the form of the abrupt discontinuity) is exhibited by the device, as seen in the L-I curves under different injection currents for various V_A settings (Fig. 2(a)). For instance, at $V_A = 0V$, the optical power surges abruptly from ~9 mW to ~40 mW at $I_G = I_{th} = ~350$ mA. This sharp turn-on behavior indicates that an intense contest is taking place between the gain and absorption mechanisms in the GS and AS, respectively [18]. When AS is reverse-biased via V_A, the total loss of the system is increased due to the enhancement in absorption loss. This absorption loss becomes more prominent with higher V_A values and increases g_{th} of the device. Consequently, higher V_A values resulted in stronger amplified spontaneous emission (ASE) from the GS. Nonetheless, this strong ASE is required to generate a considerable gain high enough to bleach this increased total loss of the system and attain the onset of lasing. Hence, higher ASE levels are observed in Fig. 2(a) at higher V_A values. Nonetheless, before the sharp turn-on point, the gain in the GS is being dominated by the enhanced system loss. However, when enough carriers are being injected in the GS to topple the system losses (*i.e.,* loss = gain = g_{th}), the whole cavity breaks through into stimulated emission region, causing the drastically steep surge in the optical power observed as the sharp turn-on in Fig. 2(a) [16].

When comparing the cases of $V_A = 0V$ and $VA = −0.8V$ in Fig 2(a), it is observed that the onset of stimulated emission is at a higher optical power value for the larger negative V_A setting. This is a result of the fact that a delayed breakthrough into stimulated emission occurs due to the elevated system g_{th}, exhibited for that V_A setting. In other words, when the whole cavity eventually achieves stimulated emission, it does so at a higher influx of carriers due to the elevated I_G value causing the optical power to abruptly higher, in turn. Hence, the height of the sharp turn-on at $V_A = 0V$ is lower compared to the $V_A = −0.8V$ setting. However, when examining the $V_A = −1.6V$ case, it is apparent that the optical power at the onset of stimulated emission is lower compared to the other two cases. This suggests that at such a high reverse bias voltage across the AS, the introduced losses in the system become too much thus quenching $d\eta_d/dI$, resulting ultimately in a reduced stimulated emission power. This becomes clearer when comparing the stimulated emission optical power at any I_G between the three V_A settings where higher negative

V_A values are associated with lower optical powers due to the introduced losses in the system and decreased $d\eta_d/dI$. In other words, higher V_A values yields in high optical power in the form of ASE and a lower onset of stimulated emission, where both contribute to the height of the sharp turn-on jump.

Next, the tunability of the lasing emission of the two-sectioned QD-LD is investigated at a current injection of $1.1I_{th}$. Fig. 2(b) depicts the emission spectra of the device under $V_A = 0, −0.8,$ and −1.6 V values. A gradual blue shift in the central emission wavelength in addition to a progressive bandwidth broadening, as V_A is swept from 0 V to −1.6 V, is observed. Both of these trends are summarized in Fig. 2(c) that shows the central wavelength blue shift from ~1611.2 nm (at $V_A = 0V$) to ~1601.9 nm (at $V_A = −1.6V$) while the 3dB bandwidth increased from ~7.4 nm to ~10.1 nm. This translates to a total continuous blue-shifted tunability of ~9.3 nm with ~2.7 nm in bandwidth enhancement. This is attributed to the increased participation of higher transition energies from the available dispersive energy states of quantum dashes associated with the intense surge of carriers that is required to overcome the enhanced losses in the system with higher negative V_A values. Furthermore, while stimulated emission takes place from quantum dash ensembles of both smaller and larger average heights (higher and lower transition energies), with larger dashes dominating as a result of photon re-absorption from the shorter dashes, in the low loss system, however, with higher negative V_A the shorter dashes now could sustain lasing while feeding the larger dashes simultaneously with increased flow of carriers (rise in threshold current). This is not unlikely in such an inhomogeneous active medium where shorter dashes possess dot-like features with a lower modal gain compared to dashes with larger average height dashes with comparatively larger modal gain [14]. This ultimately resulted in both blue shifting as well as 3dB emission broadening of the device.

Thereafter, a current injection $I_G = 1.5I_{th}$ was used to pump the GS at different V_A values in order to investigate the effect of higher current injection on the spectrum tunability and bandwidth broadening. To that end, Fig. 2(d) summarizes the maximum wavelength tunability of the two-sectioned QD-LD at both I_G settings of $1.1I_{th}$ and $1.5I_{th}$. In terms of 3dB bandwidth, the $I_G = 1.5I_{th}$ case showed a much prominent broadening effect on the 3dB bandwidth as it increased from ~8.9 nm at $V_A = 0V$ to ~14.6 nm at $V_A = −1.6V$ (~5.7 nm broadening) compared to the ~2.7 nm broadening that was witnessed in the $I_G = 1.1I_{th}$ case. In other words, not only do higher I_G values result in greater 3dB bandwidth, but they also enable a higher degree of bandwidth broadening with increased V_A across the AS. This enhanced broadening is again ascribed to the extra surge of carriers with higher I_G values to compensate the increased loss of the system with greater negative V_A values, combined with the dominant simultaneous emission from the dispersive short and large average height dash ensembles of the intentionally inhomogeneous system, as discussed above.
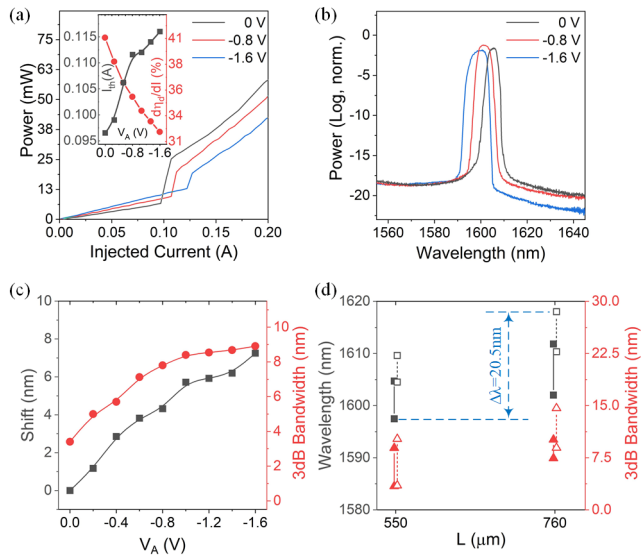
FIGURE 3. (a) The L-I curves of a two-sectioned QD-LD of a cavity length 550 μm under different reverse-bias V$_A$ values and a temperature of 14°C. The inset shows a summary of the variation in Ith and dη_d/dI as functions of V$_A$. (b) The corresponding emission spectra at a current injection of 1.1I$_{th}$ under V$_A$ values of 0, −0.8, and −1.6 V. (c) The blueshift of the central wavelength and 3dB bandwidth exhibited by the lasing spectra as a function of V$_A$. (d) A summary of the total wavelength tunability and bandwidth broadening at a current injection of 1.1I$_{th}$ (solid line) and 1.5I$_{th}$ (dashed line) for a cavity length of 550 μm and 760 μm at a fixed L$_a$/L=∼13%.

On the other hand, a smaller wavelength tunability of ∼7.7 nm is observed at the higher I$_G$ value, between V$_A$ settings of 0 V and −1.6 V, compared to ∼9.3 nm wavelength tunability that is seen at the lower I$_G$ counterpart. This is possibly due to the device junction heating as a result of high pumping of carriers that, in turn, decreases the effective band transition energies of the active region. Ultimately, this has the opposite effect of the blue shifting that occurs with higher negative V$_A$ values and counters its impact, thus limiting the total observed wavelength tunability. On the other hand, at higher injection currents, the active region temperature rise may also assist in uniformly distributing the carriers across the active region, thus aiding in emission bandwidth broadening at higher currents. With that said, a total wavelength-tuning window of ∼16 nm (∼1601.9 - 1617.9 nm) is realized (see Fig. 2(d)) by utilizing both V$_A$ and I$_G$ as tuning parameters.

2) EFFECT OF CAVITY LENGTH

Next, the effect of the cavity length on the lasing and spectral characteristics of the two-section QD-LD for a fixed L$_a$/L ratio is studied. As such, Fig. 3(a) shows the L-I curves for different V$_A$ settings of QD-LD with a cavity length of L=550 μm, corresponding to L$_a$/L=∼11-13% that is similar to 760 μm device which was investigated earlier. Similar to the longer cavity length device, the shorter 550 μm device displayed an increase in I$_{th}$ and a decrease in dη_d/dI for higher negative V$_A$ values. The inset of Fig. 3(a) summarizes

both trends as functions of V$_A$ showing that I$_{th}$(dη_d/dI) increased (decreased) from ∼96 mA (∼40%) to ∼116 mA (∼32%) as V$_A$ was swept from 0 V to −1.6 V. This translates to a ∼20% increase (∼8% decrease) in I$_{th}$(dη_d/dI) in the case of the 550-μm device compared to the corresponding much higher ∼63% increase (∼12.5% decrease) in the case of the 760-μm long device, possibly due to the less loss (due to small active region volume) introduced in the smaller AS shorter cavity length devices. The impact of this added loss with high negative V$_A$ is such that it does not significantly increase the total system loss, unlike the case of longer devices (with exhibits comparatively larger active region volume). Furthermore, comparing both cavity length devices under any fixed V$_A$ value indicates that the shorter device displays better lasing characteristics in terms of both I$_{th}$ and dη_d/dI compared to longer devices, which is a typical characteristic of FP semiconductor lasers.

In terms of threshold current densities, the longer 760-μm device showed J$_{th}$ = 15.35kA/cm^2 while the shorter 550-μm diode displayed J$_{th}$ = 5.8 kA/cm^2. At first glance, this comes counterintuitive to typical semiconductor laser characteristics where shorter cavities are generally associated with higher threshold current densities when compared to longer cavities of the same structure. However, here in this case, due to the two-sectioned nature of the devices and the associated contest between the gain and reabsorption phenomena, the threshold (onset of stimulated emission) is heavily governed by the sharp turn-on behavior, and its location. As such, since the negative bias across the AS was shown earlier to have less impact on degrading the lasing characteristics of the shorter device compared to the longer one due possibly to change in active region volumes of AS and GS, this resulted in significantly easier attainability of onset of stimulated emission by shorter cavity length device (97 mA at V$_A$ = 0V) when compared to the longer device (350 mA at V$_A$ = 0V).

Nonetheless, in terms of the spectral characteristics and wavelength tunability, Fig. 3(b) shows the emission spectrum of the 550-μm long device at a current injection of 1.1I$_{th}$ and a temperature of 14°C under V$_A$ values of 0, −0.8, and −1.6 V. Much like the longer 760-μm device, higher V$_A$ reverse biasing results in more blue shifting of the emission central wavelength as well as broadening of the 3dB bandwidth. Fig. 3(c) summarizes the exhibited blue shift in the central wavelength and 3dB bandwidth for this device as a function of V$_A$ at 1.1I$_{th}$. In terms of tunability, the shorter cavity length device showed a smaller blue shift value of ∼7.3 nm when compared to ∼9.3 nm tunability that was obtained from the 760-μm device. This is attributed to the lesser degree of inhomogeneity, which is the crucial factor in achieving the wavelength tunability here, in the smaller active region volume shorter device, as discussed earlier.

On the other hand, although the shorter 550-μm device showed a much narrower 3dB bandwidth of ∼3.4 nm when compared to the 3dB bandwidth of longer device (∼7.4 nm) at V$_A$ = 0 V, the shorter device, however, exhibited a much higher degree of bandwidth broadening (∼5.5 nm increase)

when V_A was increased to -1.6 V whereas the longer device witnessed a corresponding ~ 2.7 nm increase in the broadening of 3dB bandwidth. This could be due to the comparatively smaller I_G associated with 550 μm cavity device compared to the longer cavity device, and with accompanying the trivial rise in junction temperature. Hence, the possibility of attaining simultaneous lasing from short as well as large average height dash group is higher in shorter cavity length devices even with carrier feeding mechanism in place (i.e., photons of shorter dash group re-absorbed by larger dash ensemble) and with slight support of uniform carrier distribution across the active region via thermionic emission. The longer devices, on the other hand, experience more junction heating because of larger I_G operation compared to shorter length device. Therefore, besides improved carrier distribution across the active region evenly, thereby broadening the emission bandwidth with increasing current injection (Fig. 2(d)), the thermionic emission may also promote carrier escape from shallow band transition energy associated with dashes of shorter average-height, thus reducing the overall emission bandwidth when compared to shorter length devices, as observed in Fig. 3(c). Moreover, it is noteworthy to mention here that the effect of this thermionic carrier escape was not visible in Fig. 2(d), which has to be the case since the comparison of different I_G values was performed on a fixed 760-μm long device.

Thereafter, the spectral characteristics of L=550 μm device are obtained with I_G increased from $1.1I_{th}$ to $1.5I_{th}$, and the results of both these injection currents are summarized in Fig. 3(d) alongside 760 μm long device with both devices exhibiting a fixed $L_a/L=\sim 11$-13% ratio. The I_G settings of 550 μm device at $1.1I_{th}$ (solid lines) and $1.5I_{th}$ (dashed lines) depict much like the longer device. Increasing I_G resulted in small wavelength tunability with more 3dB bandwidth broadening in the shorter cavity length device, albeit to less severity. It is worth mentioning at this point that a total tunability of ~ 12 nm is achieved by the 550-μm device if V_A and I_G are utilized as tuning parameters, compared to ~ 16 nm continuous wavelength tunability that was attainable in the longer device. Furthermore, as illustrated in Fig. 3(d), utilizing cavity length as another tuning parameter, besides V_A and I_G, can yield an overall wavelength shift between 1597.5 nm and 1618.0 nm corresponding to a total tunability of 20.5 nm, which to our knowledge is the largest continuous tunability range in the mid L-band, thanks to the chirped structure's high degree of active region inhomogeneity.

3) EFFECT OF ABSORBER LENGTH
The impact of varying AS length L_a at a fixed cavity length is investigated on L=920 μm rather than 760 μm as the former device provides a large degree of freedom in changing the L_a value, and hence L_a/L ratio. Fig. 4(a) shows the L-I characteristics of the two-sectioned QD-LD at different L_a/L values, viz. 25, 35, and 50%, under a fixed reverse bias voltage of $V_A = -1$ V (solid lines). In general, while $V_A = -1$ V, longer absorber sections resulted in higher I_{th},
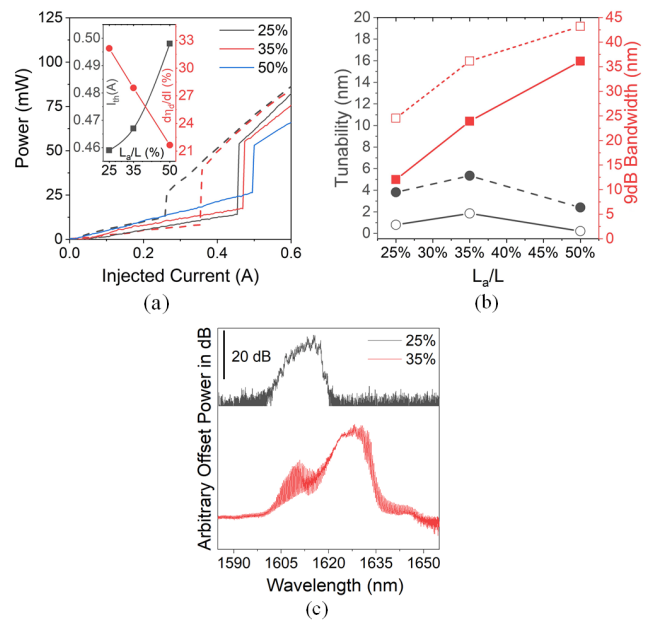

FIGURE 4. (a) The L-I curves of three 920- μm long two-sectioned QD-LDs with L_a/L values of 25, 35, 50%, at $V_A = -1$V (solid line), and when no voltage is applied across the AS (dashed line). The inset shows a summary of the variation in Ith and $d\eta_d/dI$ as functions for the different L_a/L ratios. (b) The 9dB bandwidth and blue shift of 3dB central wavelength, extracted from their emission spectra at $1.1I_{th}$ (solid lines) and $1.5I_{th}$ (dashed lines). (c) The emission spectra of the L_a/L=25% and 35% devices, when no voltage is applied across the AS, at a current injection of $1.1I_{th}$ showing the asymmetric profile.

lower $d\eta_d/dI$, and hence less optical power while the sharp turn-on behavior is observed across all cases but at different points and different levels of steep discontinuity. The inset of Fig. 4(a) summarizes the effect on I_{th} and$d\eta_d/dI$ with changing L_a/L value where the former showed an exponential rise from ~ 460 mA to ~ 495 mA while the latter exhibited a near-linear decline from $\sim 32.5\%$ to $\sim 21.5\%$. This overall degradation in the L-I characteristics can be explained by the more losses introduced in the system as the AS becomes longer, at the expense of shorter GS length, especially with higher negative V_A values. Another consequence of this is the stronger ASE (higher optical power before the sharp turn-on) as L_a/L becomes larger that is due to the competition between the overall gain and loss of the system to achieve lasing onset, as discussed in the previous sections. In general, as AS gets longer at the expense of shorter GS, the ASE of the system, under high V_A settings, becomes even more prominent since the increased system loss causes the ASE, and hence gain, to increase steadily to reach the threshold. Moreover, the reduced GS length, and thus limited modal gain, explains why the stimulated emission regime (lasing optical power), as well as the steep turn-on discontinuity, are weaker in the case of larger L_a/L compared to devices with smaller L_a/L values for any given I_G and V_A settings. This postulation is more solidified when analyzing the case where the AS is left unbiased (i.e., V_A an open circuit), which is depicted in Fig 4(a) by the dashed lines. In this case, also, smaller L_a/L ratios displayed a stronger stimulated

emission (lasing optical power) at fixed current injection, due to the longer GS (larger active region volume) and associated larger gain. More strikingly, on the contrary to the case of $V_A = -1V$, the unbiased AS case showed a stronger ASE in the smaller L_a/L device due to comparatively less system loss, thus achieving threshold gain and hence stimulated emission at much earlier injection current, thereby decreasing the abrupt discontinuity. Similarly, at larger L_a/L ratio of the unbiased AS case, the steady increase in gain due to reduced GS section results in attaining onset of lasing at higher current injection level but around similar ASE optical power level of smaller L_a/L ratio device, thus translating into large tun-on discontinuity.

In terms of the emission spectrum, Fig. 4(b) shows the witnessed blue shift in the central wavelength alongside the 9dB bandwidth for the three cases of L_a/L=25, 35, and 50% at two current injection values of $1.1I_{th}$ (solid lines) and $1.5I_{th}$(dashed lines) for the case of $V_A = -1V$. In this particular analysis, the 9dB bandwidth was adopted to truly represent the spectrum bandwidth rather than 3dB bandwidth. This was done owing to the highly asymmetric-top profile of the lasing spectra at larger L_a/L ratio devices, and for illustration purposes, Fig. 4(c) shows the case of unbiased AS case for the L_a/L=25, 35% devices wherein an asymmetric spectral nature is relatively apparent. Referring back to Fig. 4(b), a substantial increase in emission bandwidth is observed with larger L_a/L ratios (also depicted by Fig. 4(c) for unbiased AS case). For instance, the 9dB bandwidth increased from ~12 nm (~24.5 nm) for the L_a/L=25% device to ~35.1 nm (~43.2 nm) for the L_a/L=50% device under $V_A = -1$ V and I_G =1.1I_{th} (I_G =1.5$_{th}$). In general, a bandwidth enhancement of ~2 times is observed at both injection currents and any L_a/L ratio. This is again ascribed to simultaneous emission from shorter as well as larger average height dash ensembles at large L_a/L ratio while carrier feeding mechanism is active, to compensate for the increased loss of the system, hence translating to a broader lasing emission bandwidth.

In terms of the tunability of the lasing emission spectrum (*i.e.,* central wavelength blue shift at 3 dB points), both current injections followed similar trend across the three L_a/L values while achieving a maximum blue shift of ~5.3 nm and ~1.9 nm over the device with L_a/L=35% for the 1.5I_{th} and 1.1I_{th} cases, respectively. We postulate that the device junction heating at high current injections at large L_a/L devices may results in a redshift of the emission spectrum (effective transition energy shrinkage of the dashes) that counters the blue shift attempted by the reversely biased AS. In other words, optimizing the device's active region design to mitigate junction heating is crucial in a two-sectioned device with large L_a/L values to obtain a wide range of wavelength tunability.

4) OPTICAL BISTABILITY

The term optical bistability in laser devices is used to indicate hysteresis phenomenon witnessed in the L-I characteristics if it depends on the direction of current injection into
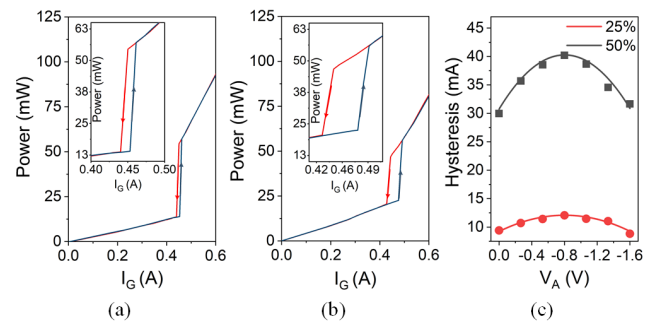

FIGURE 5. The L-I curves of 920-μm long QD-LDs with L_a/L= (a) 25% and (b) 50%, at $V_A = -0.8$ V, demonstrating the optical stability in the form of the counter-clockwise hysteresis loops. The insets show a close-up image of the hysteresis loop in each case. (c) The measured hysteresis loop width for both device as a function of V_A.

the laser device, being upward (small to large) or downward (large to small). Optical bistability has been attracting attention in many applications such as fast optical switching, next-generation optical networks, optical memory components, and optical modulation. Traditionally, optical bistability has been observed in fiber lasers and external cavity lasers [19], [5]. Nevertheless, it becomes more attractive to achieve optical bistability in monolithic compact semiconductor lasers in terms of cost, integrability, size, and flexibility. Recently, [20] reported the observation of optical bistability in quantum dot lasers emitting at 1300 nm, and from two-section semiconductor laser devices with InGaAs/GaAs quantum-dot active region [21]. Optical bistability in C-band QD-LD has also been observed [22]; however, the device was operated at a very low temperature ($-43°C$) to see this phenomenon unlike in this work wherein we observed the hysteresis in the L-I characteristics at near room temperature and in mid-L-band wavelength emitting QD-LD.

In the previous sections, the observed sharp turn-on behavior in the L-I curves showed strong bistability, which is found to be across all the tested two-sectioned QD-LD (Fig. 2(a), Fig. 3(a), and Fig. 4(a)). Hence, a more detailed analysis is presented here with the L-I curve being obtained while sweeping the injection current in an upward and then downward direction, for the three 920-μm long QD-LDs with L_a/L ratios of 25 and 50%. As such, the corresponding Fig. 5(a) and Fig. 5(b) depict the obtained results at $V_A = -0.8$ V, demonstrating sharp optical bistability witnessed by this two-sectioned QD-LD, as evident by the counter-clockwise hysteresis loop [23]. The insets of Fig. 5(a) and Fig. 5(b) show a magnified image of the hysteresis loops of each of the L_a/L=25% and 50% cases with a width of 12 and 40 mA, respectively. In other words, for a fixed cavity length, longer absorber sections translate to a higher degree of optical bistability and ascribed to the more intense contest between the gain and absorption media in the GS and AS, respectively. However, due to the higher losses taking place in the AS, the height of the hysteresis loops becomes smaller, as a result of higher ASE, as L_a/L increases. This is consistent with the L-I characteristics of Fig. 4(a).

To further investigate the effect of AS, the hysteresis loop widths were obtained for both devices at different V_A values and are plotted in Fig. 5(c) showing a near parabolic profile for both devices. Initially, increasing the negative V_A values resulted in hysteresis loop width enhancement, from 30 mA (9 mA) at $V_A = 0$ V to a maximum of 40 mA (12 mA) at $V_A = -0.8$ V for the $L_a/L=50\%$ ($L_a/L=25\%$) device. However, beyond that point, the width of the hysteresis loop decreased to 31.5 mA (8.8 mA) at $V_A = -1.6$ V. This suggests that the degree of optical stability exhibited in these two-sectioned structures can be tuned and manipulated by biasing the AS with the appropriate value to achieve the optimum hysteresis width for the desired application. For instance, in switching operations, by biasing the QD-LD in the middle of the hysteresis loop while direct modulating the GS with on-off keying, the device could be alternately turned off (spontaneous emission region) and on (stimulated emission region). It is to be noted that optical bistability in this work is observed without the aid of additional components such as resistive load, thus making it more attractive for practical applications, while in literature, this phenomenon is observed on laser diodes with [19] and without [20] resistive loads.

B. MULTI-SEGMENTED QD-LD AS SPECTRAL SHAPER

The broadband nature of the QD-LD is owed to the inhomogeneous active medium due to the intentional high variance in the sizes of the grown dashes. However, this inhomogeneity results generally into an asymmetric-top profile of the lasing emission spectrum, as the case in Fig. 4(a). This might limit the employment of this new class of QD-LD in optical communications, as additional components such as gain-flattening filters would be required. Hence, in the following section, we demonstrate the possibility of shaping the broad lasing emission profile of the QD-LD with a two-sectioned or segmented device configuration.

To that end, the L-I characteristics of a single section laser diode of a cavity length of 920 μm were obtained that exhibits a uniform injected current density distribution across the device and is equivalent to the two-sectioned device with both sections displaying uniform injected current-density. In this analysis, we employed QD-LD with $L_a/L=35\%$, and at pulsed current injection with two duty cycles, namely 0.2% and 1% with a 0.5-μs pulse width, were adopted to bias. Fig. 6(a) shows the obtained L-I curve for both duty cycles, where the smaller duty cycle case showed less exhibited losses in the active region evident by the higher slope efficiency when compared to the large duty cycle case. Thereafter, non-uniform injection current-density distribution across both segments was investigated. This was carried using I_{G1} to pump the GS1 while a different current source (I_{G2}) was used to bias the GS2 (that was the AS of the recent analysis of tunable laser). Both current sources were used to bias both sections simultaneously to achieve different current-densities within each section while keeping the total injected current (or current density) throughout the whole
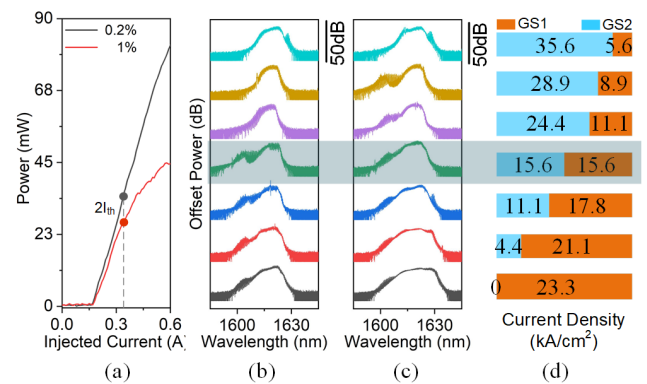

FIGURE 6. (a) The L-I curves of 920-μm long QD-LD when biased as single section, operating under two pulsed current injections with duty cycles of 0.2% and 1%, and 0.5 μs pulse width. The progressive transformation in the emission spectrum of 920-μm long two-segmented QD-LD at various current density distributions in the two sections GS1 and GS2 for the (b) 0.2% and (c) 1% duty cycle cases, and at a fixed injection current of $2I_{th} = 370$ mA. (d) The current density distributions of the GS1 and the GS2 for each corresponding spectrum of (b) and (c). The grey shaded area is the case of uniform current density distribution across the laser, representative of a single section device lasing emission curve.

device fixed at $2I_{th} = 370$ mA, where I_{th} here is that of the L-I curves of Fig. 6 (a), *i.e.,* the uniform case. Initially, only the GS1 was biased with the whole $2I_{th}$ current corresponding to a current density of $J_{G1} = 23.3$ kA/cm^2 while the GS2 was left unbiased ($J_{G2} = 0$ kA/cm^2). Then, while keeping the total aggregate current throughout the whole device fixed at $2I_{th}$, the current density of the GS1 was gradually decreased while steadily increasing the current density of the GS2. This is done to investigate the effects of non-uniform carrier-density injection on the highly inhomogeneous quantum-dash active region and hence its emission spectrum, when compared to a uniform carrier-density injection. Fig. 6(b) and Fig. 6(c) shows the progressive transformation in the emission spectrum of the QD-LD at various current-density distributions for the 0.2 and 1% duty cycle cases, respectively. Fig. 6(d), on the other hand, illustrates the current density distributions of the GS1 and the GS2 sections for each adjacent spectrum where the length of the colored bars roughly represents the carrier-density concentration of the GS1 and the GS2. Furthermore, the highlighted case in grey color represents the case of equal current density in both segments, which translates to a uniform carrier-density distribution (15.6 kA/cm^2) across the whole device and representative of a single section device. Hence, this case is taken as a reference in the subsequent analysis.

By analyzing Figs. 6 (b)-(d), several observations could be drawn on the emission spectra of the QD-LD. Starting from the highlighted uniform reference case, with increasing current density in the GS1 (*i.e.,* moving downwards in Figs. 6 (b)-(d) from the reference spectrum), wavelength components at the short wavelength side of the spectra gradually disappear in the smallest duty cycle case indicating some quantum dashes (particularly ones of smaller heights) in the active region unable to reach stimulated emission.

This signifies that these wavelength components were being emitted from dashes residing in the GS2, and with the shift in carrier density of GS1, became more concentrated in GS1 and seized to lase. This suggests that GS1 dictates the spectral behavior of the system in this case compared to GS2. Furthermore, although dashes of similar sizes are likely to exist in the GS1 as well, these short-wavelength components remained absent in the emission spectrum as the current density increases, particularly for a 0.2% duty cycle case. This is attributed to the carrier feeding via optical pumping mechanism. In other words, when the current density in the GS1 is high enough, the photons generated by the dash group with smaller average heights (shorter wavelength components) gets absorbed by the dash ensemble with larger heights (medium and long-wavelength components) and hence struggle to achieve population inversion and to lase. However, this attribution does not hold for the higher 1% duty cycle case (Fig. 6 (c)). As the current density of GS1 increases, the appearance of the shorter wavelength components persists, suggesting the dash ensembles with smaller height sustaining lasing. This might be ascribed to higher duty cycle operation that inherently associates with a higher junction temperature enabling a relatively uniform distribution of carriers across dispersive size dashes with a high probability of maintaining stimulated emission with the aid of thermionic emission process.

Conversely, with increasing current density in the GS2, (*i.e.,* moving upwards in Figs. 6 (b)-(d) from the reference case), the peak wavelength of the spectra, as well as the short and long wavelength components, exhibits a more apparent blue shift compared to the observed red shift in 0.2% duty cycle case. This again suggests domination from GS2 compared to the GS1 of the laser device. Furthermore, a much more significant vanishing of the shorter wavelength components (associated with the smaller height dash ensemble) with increasing current density in the GS2 is observed. Previously, we attributed the large duty cycle with comparatively high junction temperature responsible for achieving relatively uniform carrier distribution across the dashes in aiding stimulated emission from short height dashes as well. In the case of GS2, however, too large junction temperature rise prevents fast heat dissipation from the active region due to small volume, and as a consequence can have the opposite effect *i.e.,* large carrier leakage or spillover from quantum dashes of smaller heights that are generally shallower and less confined [24]. As a result, the emission coverage becomes considerably narrower when the carrier density increases in the GS2. The most noteworthy phenomenon that can be observed in Figs. 6 (b)-(d) is how manipulating the current density distribution between the two sections of the QD-LD with respective biasing currents circuit transforms the shape of the spectrum. Most remarkably, shifting the current density towards either the GS1 or the GS2 results in a much more symmetrical spectrum with a flatter top surface when compared to uniform current injection that results in non-symmetrical spectral shapes that are associated with highly inhomogeneous quantum structures. In particular, increasing (or shifting) the carrier density of GS1 also leads to broader 3dB bandwidth. For instance, a nearly flat-top spectral shape with wider lasing 3dB bandwidth of ~20 nm is achieved at $J_{G1} = 23.3$ kA/cm^2 compared to the reference case of ~7 nm at 1% duty cycle. Such a broad and symmetric lasing profile is desirable in a multitude of applications, mainly WDM systems and biomedical sensing and imaging. Moreover, this provides a potential improvement to the asymmetric-top profiles associated with these two-sectioned highly inhomogeneous devices while operated as tunable lasers.

IV. CONCLUSION

We comprehensively investigated a two-section InAs/InP quantum-dash laser as a semiconductor tunable laser. A large blue shift wavelength tuning was observed, reaching a value of ~20 nm in the mid-L-band wavelength region with ~2 times improvement in the emission bandwidth broadening. Moreover, optical bistability is observed in the device L-I characteristics in the form of a hysteresis loop with a width of as large as 40 mA. Hence, these results underpin the potential of two-sectioned InAs/InP QD-LD as a light source in several multi-disciplinary fields of applications and optical access networks in particular. Finally, the monolithic two-segmented device was also demonstrated as a lasing spectrum shaper to attain flat top emission profiles. A substantially enhanced 3dB bandwidth of ~20 nm, from ~7 nm is achieved. These diverse investigations from two-sectioned QD-LD positions the prospect of seamless integration of tunable laser as well as spectrum shaper on a single monolithic multi-sectioned device whose both emission spectrum wavelength coverage, as well as spectral profile, could be tuned.

REFERENCES

[1] L. A. Coldren, "Monolithic tunable diode lasers," *IEEE J. Sel. Topics Quantum Electron.*, vol. 6, no. 6, pp. 988–999, Nov./Dec. 2000.

[2] J.-Y. Kim, H.-S. Cho, S.-G. Mun, H.-K. Lee, and C.-H. Lee, "High-capacity DWDM-PON using triple-contact F-P LDs," *IEEE Photon. Technol. Lett.*, vol. 23, no. 2, pp. 127–129, Jan. 15, 2011.

[3] M. Kye and C.-H. Lee, "Injection locked triple contact F-P LDs for uncooled WDM systems," *IEEE Photon. Technol. Lett.*, vol. 30, no. 2, pp. 213–216, Jan. 15, 2018.

[4] A.-H. Kim, J.-H. Park, H.-S. Cho, and C.-H. Lee, "Laser spectral envelope control using a double contact Fabry–Pérot laser diode for WDM-PON," *IEEE Photon. Technol. Lett.*, vol. 18, no. 20, pp. 2132–2134, Oct. 2006.

[5] M. Feng, N. A. Brilliant, S. T. Cundiff, R. P. Mirin, and K. L. Silverman, "Wavelength bistability in two-section mode-locked quantum-dot diode lasers," *IEEE Photon. Technol. Lett.*, vol. 19, no. 11, pp. 804–806, Jun. 1, 2007.

[6] N. A. Pikhtin, A. Y. Leshko, A. V. Lyutetskii, V. B. Khalfin, N. V. Shuvalova, Y. V. Il'in, and I. S. Tarasov, "Two-section InGaAsP/InP Fabry–Pérot laser with a 12 nm tuning range," *Tech. Phys. Lett.*, vol. 23, no. 3, pp. 214–216, Mar. 1997.

[7] D. C. Byrne, J. P. Engelstaedter, W.-H. Guo, Q. Y. Lu, B. Corbett, B. Roycroft, J. O'Callaghan, F. H. Peters, and J. F. Donegan, "Discretely tunable semiconductor lasers suitable for photonic integration," *IEEE J. Sel. Topics Quantum Electron.*, vol. 15, no. 3, pp. 482–487, 2009.

[8] S. Sakano, T. Tsuchiya, M. Suzuki, S. Kitajima, and N. Chinone, "Tunable DFB laser with a striped thin-film heater," *IEEE Photon. Technol. Lett.*, vol. 4, no. 4, pp. 321–323, Apr. 1992.

[9] K. Liu, S. X. Mu, Y. Lu, B. L. Guan, and E. Y. B. Pun, "L-band wavelength-tunable MQW Fabry–Pérot laser using a three-segment structure," *IEEE Photon. Technol. Lett.*, vol. 25, no. 18, pp. 1754–1757, Sep. 15, 2013.

[10] F. Smyth, E. Connolly, B. Roycroft, B. Corbett, P. Lambkin, and L. P. Barry, "Fast wavelength switching lasers using two-section slotted Fabry–Pérot structures," *IEEE Photon. Technol. Lett.*, vol. 18, no. 20, pp. 2105–2107, Oct. 2006.

[11] Y. Wang, Y. Yang, and J.-J. He, "Single-electrode controlled four-section coupled-cavity tunable laser," *IEEE Photon. Technol. Lett.*, vol. 25, no. 14, pp. 1340–1343, Jul. 15, 2013.

[12] J. Jin, L. Wang, T. Yu, Y. Wang, and J.-J. He, "Widely wavelength switchable V-coupled-cavity semiconductor laser with ~40 dB side-mode suppression ratio," *Opt. Lett.*, vol. 36, no. 21, pp. 4230–4232, Oct. 2011.

[13] D. I. Nikitichev, M. Cataluna, K. A. Fedorova, Y. Ding, S. S. Mikhrin, I. L. Krestnikov, D. A. Livshits, and E. U. Rafailov, "High-power wavelength bistability and tunability in passively mode-locked quantum-dot laser," *IEEE J. Sel. Topics Quantum Electron.*, vol. 19, no. 4, Jul. 2013, Art. no. 1100907.

[14] M. Z. M. Khan, T. K. Ng, C.-S. Lee, P. Bhattacharya, and B. S. Ooi, "Investigation of chirped InAs/InGaAlAs/InP quantum dash lasers as broadband emitters," *IEEE J. Quantum Electron.*, vol. 50, no. 2, pp. 51–61, Feb. 2014.

[15] B. Sartorius, M. Mohrle, S. Reichenbacher, H. Preier, H.-J. Wunsche, and U. Bandelow, "Dispersive self-Q-switching in self-pulsating DFB lasers," *IEEE J. Quantum Electron.*, vol. 33, no. 2, pp. 211–218, Feb. 1997.

[16] M. J. R. Heck, E. A. J. M. Bente, B. Smalbrugge, Y.-S. Oei, M. K. Smit, S. Anantathanasarn, and R. Nötzel, "Observation of Q-switching and mode-locking in two-section InAs/InP (100) quantum dot lasers around 1.55 µm," *Opt. Express*, vol. 15, no. 25, pp. 16292–16301, 2007.

[17] E. Alkhazraji, M. S. Alias, and M. Z. M. Khan, "Multi-stack chirped InAs/InP quantum-dash structure as a tunable laser," in *Proc. Asia Commun. Photon. Conf. (ACP)*, Hangzhou, China, Oct. 2018, pp. 1–3.

[18] E. Alkhazraji, M. Alias, and M. Khan, "Optical bistability in monolithic two-sectioned InAs/InP quantum-dash laser," in *Proc. 7th Int. Conf. Photon., Opt. Laser Technol.*, Prague, Czech, 2019, pp. 1–4.

[19] H. Kawaguchi, T. Mori, Y. Sato, and Y. Yamayoshi, "Optical buffer memory using polarization-bistable vertical-cavity surface-emitting lasers," *Jpn. J. Appl. Phys.*, vol. 45, no. 34, pp. L894–L897, Aug. 2006.

[20] X. Huang, A. Stintz, H. Li, A. Rice, G. T. Liu, L. P. Lester, J. Cheng, and M. J. Malloy, "Bistable operation of a two-section 1.3 µm InAs quantum dot laser-absorption saturation and the quantum confined stark effect," *IEEE J. Quantum Electron.*, vol. 37, no. 3, pp. 414–417, Mar. 2001.

[21] O. Qasaimeh, W.-D. Zhou, J. Phillips, S. Krishna, P. Bhattacharya, and M. Dutta, "Bistability and self-pulsation in quantum-dot lasers with intra-cavity quantum-dot saturable absorbers," *Appl. Phys. Lett.*, vol. 74, no. 12, pp. 1654–1656, Mar. 1999.

[22] P. E. Harnedy, F. Lelarge, S. Osborne, E. P. O'Reilly, and S. Joshi, "Bistability of threshold in quantum dash-in-a-well lasers," *IET Optoelectron.*, vol. 8, no. 2, pp. 94–98, Apr. 2014.

[23] E. Alkhazraji, "A multi-segment broadband quantum-dash laser diode with controllable lasing spectrum," in *Proc. Asia Commun. Photon. Conf.*, Chengdu, China, 2019, Paper M4A.255.

[24] C. L. Tan, H. S. Djie, Y. Wang, C. E. Dimas, V. Hongpinyo, Y. H. Ding, and B. S. Ooi, "The influence of nonequilibrium distribution on room-temperature lasing spectra in quantum-dash lasers," *IEEE Photon. Technol. Lett.*, vol. 21, no. 1, pp. 30–32, Jan. 1, 2009.

EMAD ALKHAZRAJI (Member, IEEE) was born in Mansoura, Egypt, in 1992. He received the B.S. and M.S. degrees in electrical engineering from King Fahd University of Petroleum and Minerals (KFUPM), Saudi Arabia, in 2014 and 2016, respectively.

Since 2016, he has been a part-time Ph.D. student with the Electrical Engineering Department, KFUPM, and a full-time Lecturer with the Department of Electrical and Electronic Engineering Technology, Jubail Industrial College (JIC), Saudi Arabia. From 2014 to 2016, he was a Research Assistant with the Electrical Engineering Department, KFUPM. His research focuses on semiconductor quantum dash lasers and their applications in optical communications.

MOHD SHARIZAL ALIAS (Senior Member, IEEE) received the B.Sc. and M.Sc. degrees in physics from the University of Malaya, in 2000 and 2005, respectively, and the Ph.D. degree in microengineering and nanoelectronics from the National University of Malaysia, in 2010. He was a Postdoctoral Researcher at the Department of Materials, University of Oxford, U.K., from 2018 to 2019. From 2013 to 2018, he was a Research Scientist at King Abdullah University of Science and Technology, Saudi Arabia. Before joining academia, he was a Principal Researcher at Telekom Malaysia Research and Development from the year 2003 to 2013. He is currently a Faculty Member of the Electrical Engineering Department, Higher Colleges of Technology, Dubai, UAE. His research focuses on the usage of nanophotonics to enhance light manipulation for photonic devices. His other research interests include semiconductor lasers and micro-/nano-fabrication process.

KHURRAM KARIM QURESHI (Senior Member, IEEE) received the B.Sc. degree (Hons.) in electrical engineering from the University of Engineering and Technology, Pakistan, in 1999, and the Ph.D. degree in electrical engineering from The Hong Kong Polytechnic University, in 2006. He is currently an Associate Professor with the Electrical Engineering Department, King Fahd University of Petroleum and Minerals (KFUPM). His research interests include tunable semiconductor and fiber-based lasers, and fiber sensors.

MOHAMMED ZAHED MUSTAFA KHAN (Senior Member, IEEE) received the B.E. degree from Osmania University, India, in 2001, and the M.S. and Ph.D. degrees in electrical engineering from King Fahd University of Petroleum and Minerals (KFUPM) and King Abdullah University of Science and Technology (KAUST), Saudi Arabia, in 2004 and 2013, respectively.

From 2014 to 2015, he was a SABIC Postdoctoral Research Fellow with Photonics Laboratory, KAUST. Since 2015, he has been an Assistant Professor of Electrical Engineering, KFUPM. His prior research involved developing numerical models for integrated optical device simulation. His current research focuses on the development of near-infrared and visible semiconductor lasers and systems for applications in optical communications. He is a member of the Optical Society of America.

• • •